Journal of Power Sources 196 (2011) 6716–6722

Contents lists available at ScienceDirect

Journal of Power Sources

journal homepage: www.elsevier.com/locate/jpowsour

Closely packed SiO_2 nanoparticles/poly(vinylidene fluoride-hexafluoropropylene) layers-coated polyethylene separators for lithium-ion batteries

Hyun-Seok Jeong, Sang-Young Lee*

Department of Chemical Engineering, Kangwon National University, Chuncheon, Kangwondo 200-701, Republic of Korea

ARTICLE INFO

Article history:
Received 11 August 2010
Received in revised form 6 November 2010
Accepted 8 November 2010
Available online 12 November 2010

Keywords:
Lithium-ion batteries
Composite separators
Ceramic coating layers
Close-packed SiO_2 nanoparticles
Thermal shrinkage
Cell performances

ABSTRACT

In an effort to improve thermal shrinkage and electrochemical performance of a separator for a lithium-ion battery, we develop a new composite separator by introducing ceramic coating layers onto both sides of a polyethylene (PE) separator. The ceramic coating layers are comprised of SiO_2 nanoparticles and polyvinylidene fluoride-hexafluoropropylene (PVdF-HFP) binders. In comparison to the dense structure of conventional nanocomposite coating layers, the ceramic coating layers are featured with close-packed SiO_2 nanoparticles, which affords a well-developed porous structure, i.e. highly connected interstitial voids formed between the nanoparticles. On the basis of this structural understanding of the composite separators, the effects of ceramic coating layers on the separator properties are investigated as a function of SiO_2 powder size. Owing to the existence of the heat-resistant SiO_2 coating layers, the composite separators show significant reduction in thermal shrinkage than the pristine PE separator. More intriguingly, in comparison to the large-sized (≈530 nm) SiO_2, the small-sized (≈40 nm) SiO_2 offers a large number of SiO_2 nanoparticles in the ceramic coating layers, high porosity contributing to facile ion transport, and small increase in the cell impedance, which consequently allows substantial improvements in cell performances as well as thermal shrinkage of the separator.

1. Introduction

Rapidly growing demand for high energy-density and high power-density lithium-ion batteries has motivated researchers to focus on the accompanying battery safety failures. In particular, from the viewpoint of suppressing internal short-circuit problems, a separator in a lithium-ion battery is considered a critical component to secure battery safety, as its major function is to physically isolate the cathode and anode so that no electrons can flow between them [1–3]. Currently, the most widely used separators in lithium-ion batteries are made of polyolefins, specifically polyethylene (PE) and polypropylene (PP). While these polyolefin-based separators offer many advantages, their poor thermal stability and mechanical strength raise serious concerns regarding the electrical isolation between electrodes, the failure of which could eventually lead to fire or explosion of cells [4,5]. In order to overcome these drawbacks of polyolefin-based separators, various separators have been proposed, including self-standing inorganic separators [6,7], nanocomposite-coated PE separators [4,8,9], nonwoven-ceramic composite separators [10], and nanofiber-based separators prepared by electrospinning [5,11,12]. Among these alternatives, the use of ceramic powders has drawn considerable attention, owing to their effectiveness in preventing thermal shrinkage and mechanical breakdown of separators.

Well-controlled nanoparticle arrangement driven by self-assembly has been extensively investigated, as an ideal starting template for the preparation of porous materials that can be used in various applications ranging from sensors to catalysts [13–15]. In contrast to conventional nanocomposites characterized by nanoparticles embedded in a polymer matrix, this approach pursues the establishment of a highly ordered nanoporous structure, where nanoparticles are close-packed and interconnected by organic binders. Exploiting this intriguing concept, in an attempt to significantly improve the thermal shrinkage and electrochemical performance of a separator, we develop a new composite separator, which is based on introduction of ceramic coating layers onto both sides of a polyethylene (PE) separator. The ceramic coating layers consist of SiO_2 nanoparticles and polyvinylidene fluoride-hexafluoropropylene (PVdF-HFP) binders. Notable features of the ceramic coating layers are close-packed SiO_2 nanoparticles, which affords a well-developed porous structure, i.e. highly connected interstitial voids formed between the nanoparticles. These ceramic coating layers are expected to substantially affect the separator properties. In this study, the effects of the ceramic coating layers

* Corresponding author. Tel.: +82 33 250 6338; fax: +82 33 251 3658.
E-mail address: syleek@kangwon.ac.kr (S.-Y. Lee).

0378-7753/$ – see front matter © 2010 Elsevier B.V. All rights reserved.
doi:10.1016/j.jpowsour.2010.11.037

on the thermal shrinkage of composite separators and the cell performances such as discharge capacity, discharge *C*-rate capability, and cyclability are investigated as a function of SiO_2 powder size (herein, 40 and 530 nm), and the results are compared with those obtained with a pristine PE separator.

2. Experimental

2.1. Preparation of the composite separators

The solution for ceramic coating layers was prepared by mixing SiO_2 (average particle size = 40 and 530 nm, Denki Kagaku) and PVdF-HFP (HFP content = 6 mol%, Arkema) in acetone as a solvent, where a ratio of SiO_2/PVdF-HFP was fixed at 90/10 (wt%/wt%). After first dissolving PVdF-HFP in acetone, a fixed amount of SiO_2 powder was added and the solution was further subjected to vigorous mixing via bead-milling for 2 h. As a coating substrate, a microporous PE separator (thickness = 20 μm, porosity = 45%, Tonen) was chosen. The coating solution was applied onto both sides of the PE separators via a dip-coating process. The separators were then dried at room temperature to evaporate acetone and further vacuum dried at 50 °C for 4 h. The final thickness of the composite separators was measured to be around 30 μm, which is thicker than that (20 μm) of the pristine PE separator. This may cause an undesirable reduction of volumetric capacity of batteries, however, which could be compensated by adjusting cell design factors. For instance, application of thinner packaging materials, thinner current collectors for electrodes, high-capacity electrode active materials, and thinner pristine PE separators (as a coating substrate) can be recommended.

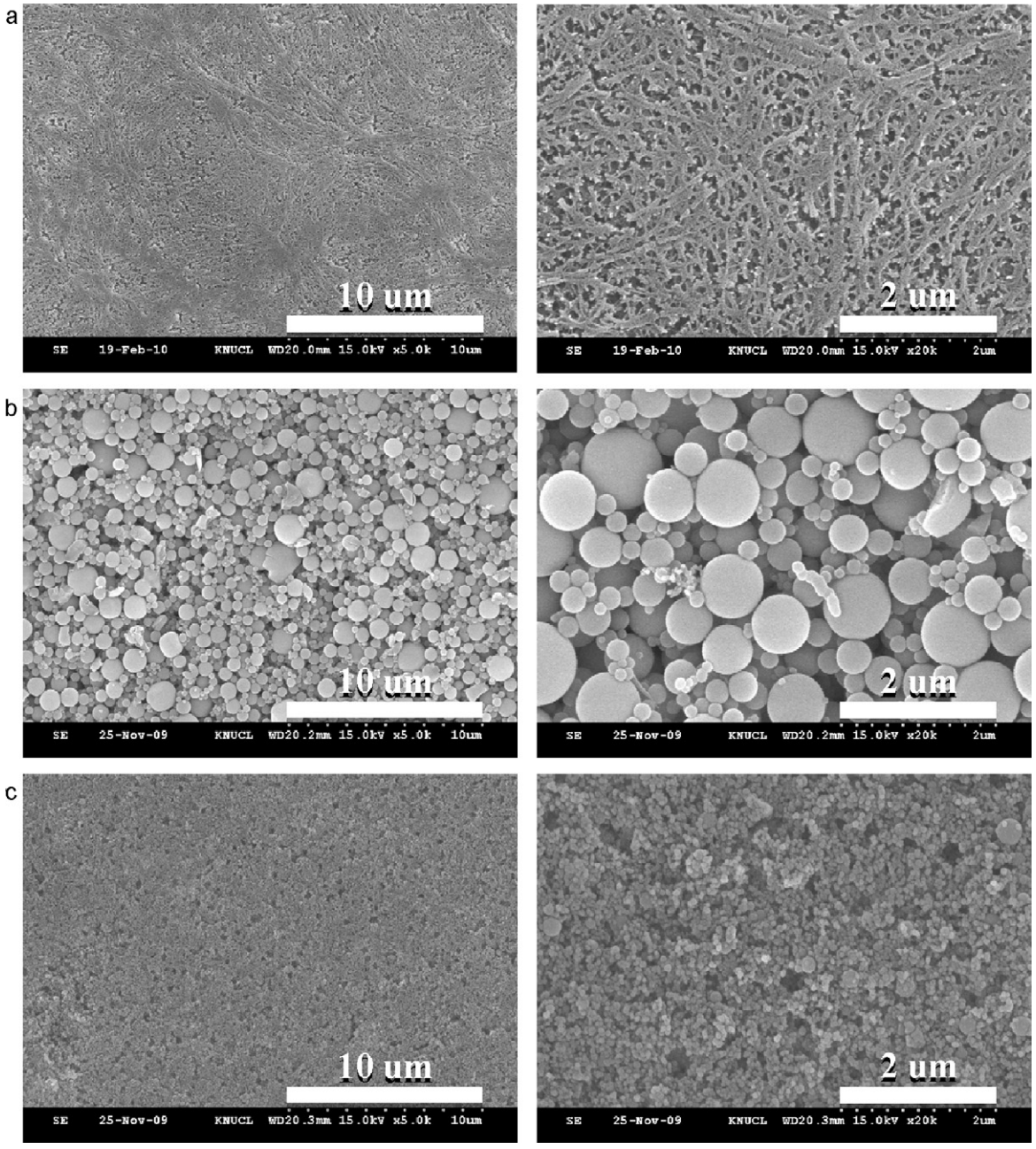

Fig. 1. FE-SEM photographs of surface morphologies for: (a) pristine PE separator, (b) 530 nm SiO_2-coated composite separator, and (c) 40 nm SiO_2-coated composite separator.

Table 1
Basic characteristics of various separators: porosity, total ionic conductance, thermal shrinkage, and number of SiO_2 particles per unit area of a ceramic coating layer.

Separator	Porosity (SiO_2 coating layer/ PE separator) (%/%)	Total ionic conductance (S)	Thermal shrinkage at 140 °C/0.5 h (%)	Number of SiO_2 particles (ea cm^{-2})
Composite separator (40 nm SiO_2)	68/45	0.61	23	1.53×10^{13}
Composite separator (530 nm SiO_2)	50/45	0.53	67	0.89×10^{10}
Pristine PE separator	–/45	0.65	92	–

2.2. Characterization of the composite separators

The surface morphology of the ceramic coating layers was investigated using a field emission scanning electron microscope (FE-SEM, S-4300, Hitachi) in the central laboratory of Kangwon National University. The porosity ($=(\rho_c - \rho_e)/\rho_c$) of the ceramic coating layers was examined by measuring their density, where ρ_c is the calculated density for a dense coating layer (assumed to be without pores) and ρ_e is the experimental density for a porous coating layer [16,17]. The thermal shrinkage of the ceramic composite separators was determined by measuring the dimensional change after being subjected to heat treatment at various temperatures for 0.5 h [9]. For measurement of the electrochemical performance, a liquid electrolyte of 1 M $LiPF_6$ in ethylene carbonate (EC)/diethyl carbonate (DEC) (1/1, v/v, Technosemi Chem) was employed. The electrochemical stability window of the separators was evaluated by a linear sweep voltammetry experiment performed on a working electrode of stainless-steel and a counter and reference electrode of lithium-metal at a scan rate of 1.0 mV s^{-1}. A unit cell (2032-type coin) was assembled by sandwiching a separator between a natural graphite anode and a $LiCoO_2$ cathode and then activated by filling it with the liquid electrolyte. All assembly of cells was carried out in an argon-filled glove box. The discharge capacities, discharge *C*-rate capability, and cyclability of the cells were examined using battery test equipment (PNE solution). The discharge current densities were varied from 0.2 (=0.76 mA cm^{-2}) to 1.0 C (=3.79 mA cm^{-2}) at a constant charge current density of 0.2 C under a voltage range between 3.0 and 4.4 V. The cells were cycled at a constant charge/discharge current density of 0.5 C/0.5 C. The AC impedance spectra of fully charged cells were obtained using a using a VSP classic (Bio-Logic) over a frequency range of 0.01 to 10^6 Hz.

3. Results and discussion

The morphologies of the composite separators are compared with that of the pristine PE separator. In contrast to the pristine PE separator (Fig. 1(a)), the composite separators (Fig. 1(b) and (c)) have unique ceramic coating layers comprising close-packed SiO_2 nanoparticles interconnected by PVdF-HFP binders. The over-

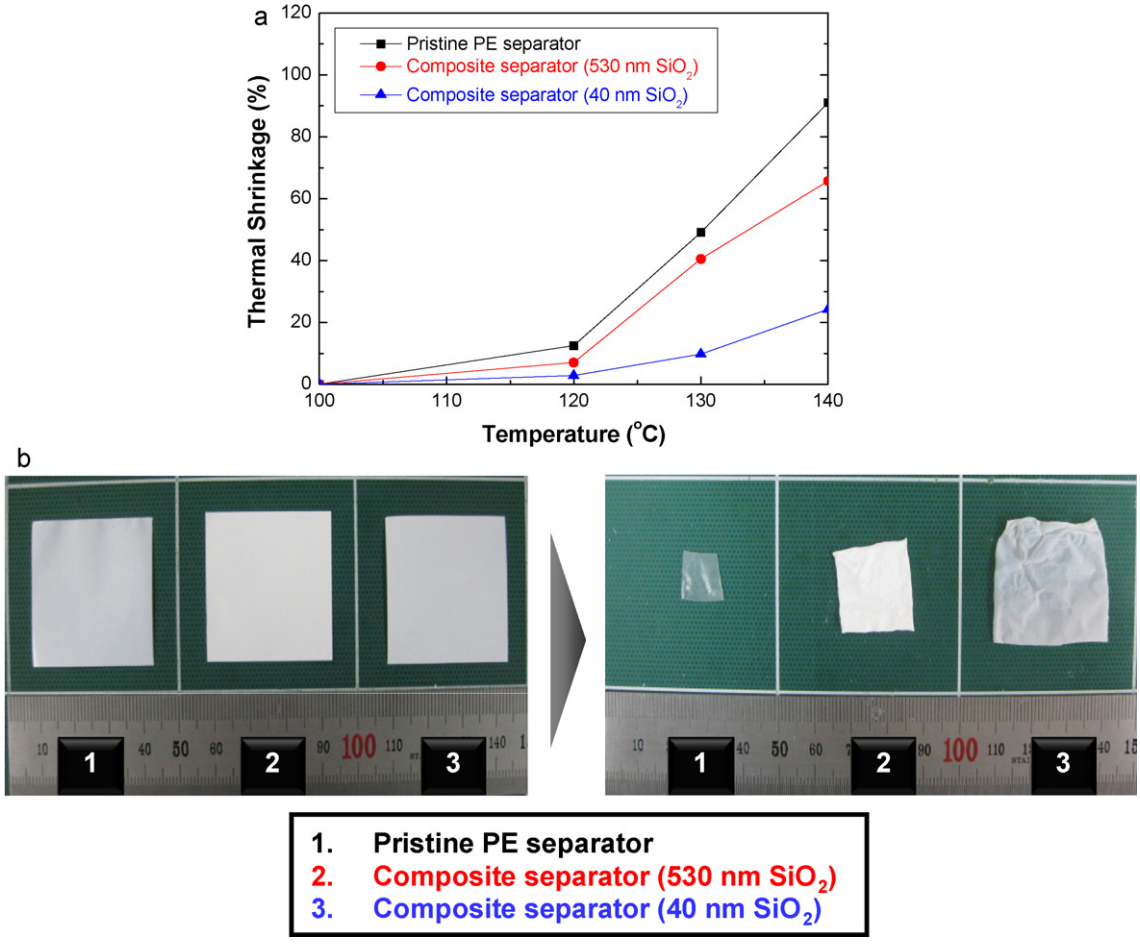

Fig. 2. (a) Thermal shrinkage of composite separators and pristine PE separator as a function of heat-treatment temperature and (b) photographs of composite separators and pristine PE separator before/after being exposed to 140 °C for 0.5 h.

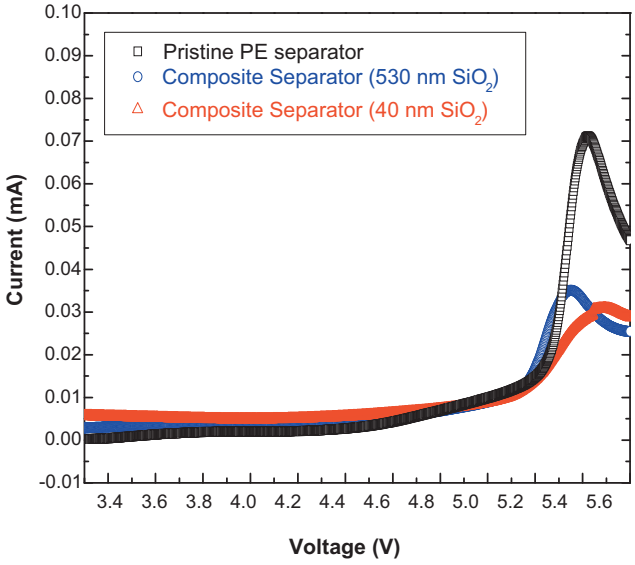

Fig. 3. Linear sweep voltammograms of composite separators and PE separator at a voltage scan rate of 1.0 mV s^{-1}.

all morphology of the ceramic coating layers is similar to the nanoparticle arrangement driven by self-assembly reported in previous studies [13–15]. These ceramic coating layers are expected to prevent the composite separators from being thermally shrunk, owing to the existence of heat-resistant SiO_2 powders. Meanwhile, in comparison with the dense structure of conventional nanocomposite coating layers [8,9], another distinct feature of the ceramic coating layers is their porous structures, i.e. well-connected interstitial voids formed between the SiO_2 nanoparticles. These porous structures will be filled with liquid electrolytes and may provide a facile pathway for ion movement, contributing to faster ion conduction than the dense structures.

Meanwhile, the comparison between Fig. 1(b) and (c) demonstrates that the porous structure of ceramic coating layers strongly depends on the SiO_2 powder size. The pore size of the 40-nm SiO_2 coating layers is much smaller than that of the 530-nm SiO_2 coating layers. In order to provide a more detailed characterization of the porous structure, the porosities of the ceramic coating layers are examined (Table 1). In comparison to the porosity (=45%) of the pristine PE separator, the porosities of SiO_2 coating layers are observed to be 50% for the 530-nm SiO_2 and 68% for the 40-nm SiO_2, respectively. This makes sure that the close-packed SiO_2 nanoparticles allow for the development of porous structures in the coating layers, which is more pronounced for the small-sized particles. The higher porosity of the 40-nm SiO_2 coating layers can be explained by considering the fact that smaller-sized particles tend to yield low tap density, indicating loose packing of the particles in a determined volume [17].

This change in the porosity of ceramic coating layers is expected to strongly affect ion transport behavior of composite separators. When separators with different thicknesses are incorporated into cells, cell performances tend to be practically influenced by total ionic conductance (=S) of separators rather than ion conductivity (=S cm^{-1}) that is normalized by separator thickness. Table 1 shows

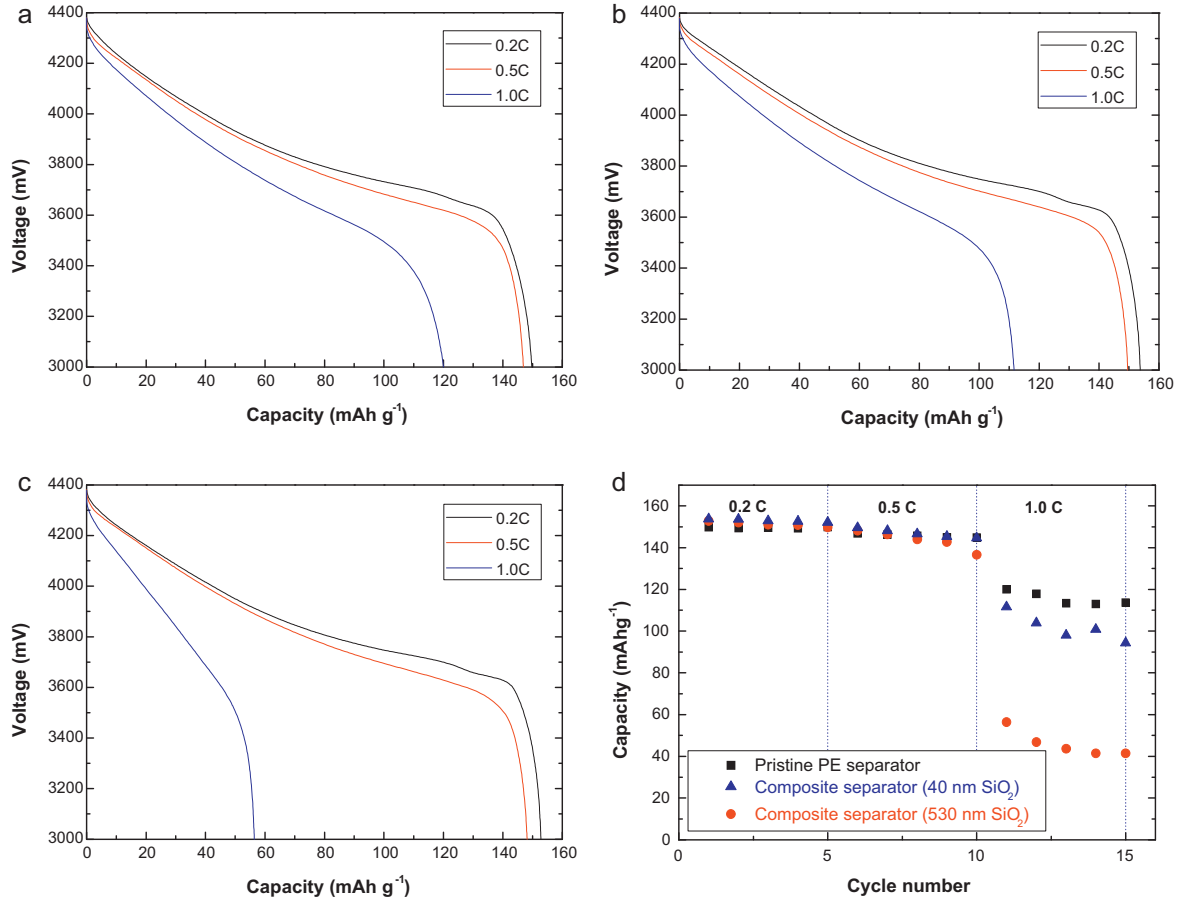

Fig. 4. Discharge profiles of cells assembled with: (a) pristine PE separator, (b) 40 nm SiO_2-coated composite separator, (c) 530 nm SiO_2-coated composite separator, and (d) comparison of discharge capacities and *C*-rate capabilities, where discharge current densities are varied from 0.2 to 1.0 C at a constant charge current density of 0.2 C under a voltage range between 3.0 and 4.4 V.

that the total ionic conductances are observed to be 0.61 S for the 40 nm SiO_2-coated composite separator and 0.53 S for the 530 nm SiO_2-coated one, while the pristine PE separator exhibits the highest total ionic conductance of 0.65 S. The relatively lower total ionic conductances of the SiO_2-coated composite separators may be due to the existence of ceramic coating layers onto the PE separator and their greater thickness (~30 μm) relative to the pristine PE separator (~20 μm), possibly causing long tortuous path for ion transport. Interestingly, the relatively higher total ionic conductance of the 40 nm SiO_2-coated composite separator than that of the 530 nm SiO_2-coated one is observed, which indicates that the total ionic conductance of the composite separators depends heavily on the porous structure, more specifically porosity (i.e., 50% for the 530-nm SiO_2 and 68% for the 40-nm SiO_2) of the ceramic coating layers.

The thermal shrinkage of the composite separators was observed by measuring their (area-based) dimensional change after being subjected to heat treatment at various temperatures for 0.5 h (Fig. 2). Since conventional PE separators have a melting point of about 135 °C and are prepared through multiple stretching processes, they easily lose dimensional stability upon exposure to high temperatures of above 100 °C. Fig. 2(a) shows that over a wide range of temperatures, the composite separators markedly suppress the thermal shrinkage compared to the pristine PE separator. This improvement in the thermal shrinkage of the composite separators is ascribed to the existence of ceramic coating layers, more specifically the close-packed SiO_2 nanoparticles. The heat-resistant SiO_2 nanoparticles are believed to effectively prevent the composite separator from being thermally shrunk. Another interesting finding is that the 40 nm SiO_2-coated composite separator exhibits greater reduction in the thermal shrinkage than the 530 nm SiO_2-coated one. Fig. 2(b) shows photographs of separators before/after exposure to a temperature of 140 °C for 0.5 h. The thermal shrinkages of the separators are observed to be 23% for the 40 nm SiO_2-coated composite separator and 67% for the 530 nm SiO_2-coated one, in comparison to 92% for the pristine PE separator. This noticeable improvement in the thermal shrinkage of the 40 nm SiO_2-coated composite separator is attributed to the higher number of SiO_2 particles in the ceramic coating layers. Under the assumption that SiO_2 particles are spherical and have a uniform particle size distribution, the number of SiO_2 particles per unit area of a ceramic coating layer can be calculated by measuring the weight of the ceramic coating layer and the density (=2.20 g cc^{-1} for SiO_2 and 1.76 g cc^{-1} for PVdF-HFP) of the components. Table 1 shows that the number of SiO_2 particles is calculated to be 1.53×10^{13} ea cm^{-2} for the 40-nm SiO_2 coating layer, a value considerably higher than 0.89×10^{10} ea cm^{-2} for the 530-nm SiO_2 one. This demonstrates that the number of SiO_2 particles in the ceramic coating layers could critically affect the thermal shrinkage of composite separators.

The electrochemical stability window of the composite separators was observed from the linear sweep voltammograms. Fig. 3 shows that the electrochemical stability of the composite separators is comparable to that of a commercialized PE separator and

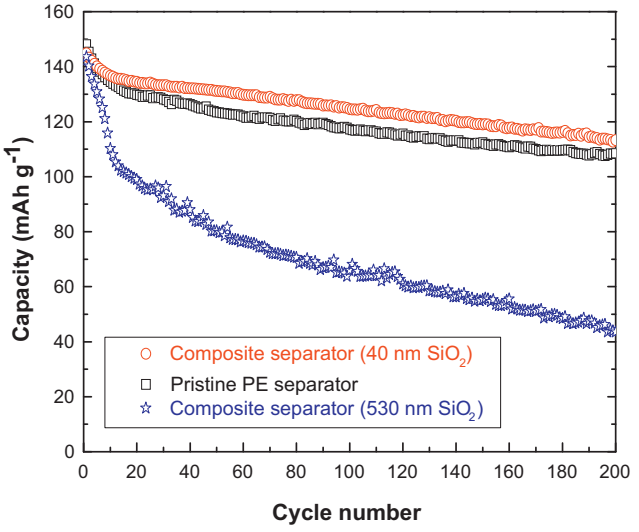

Fig. 5. Cycle performance of cells assembled with various separators, where cells are cycled at a constant charge/discharge current density (0.5 C/0.5 C) under a voltage range between 3.0 and 4.4 V.

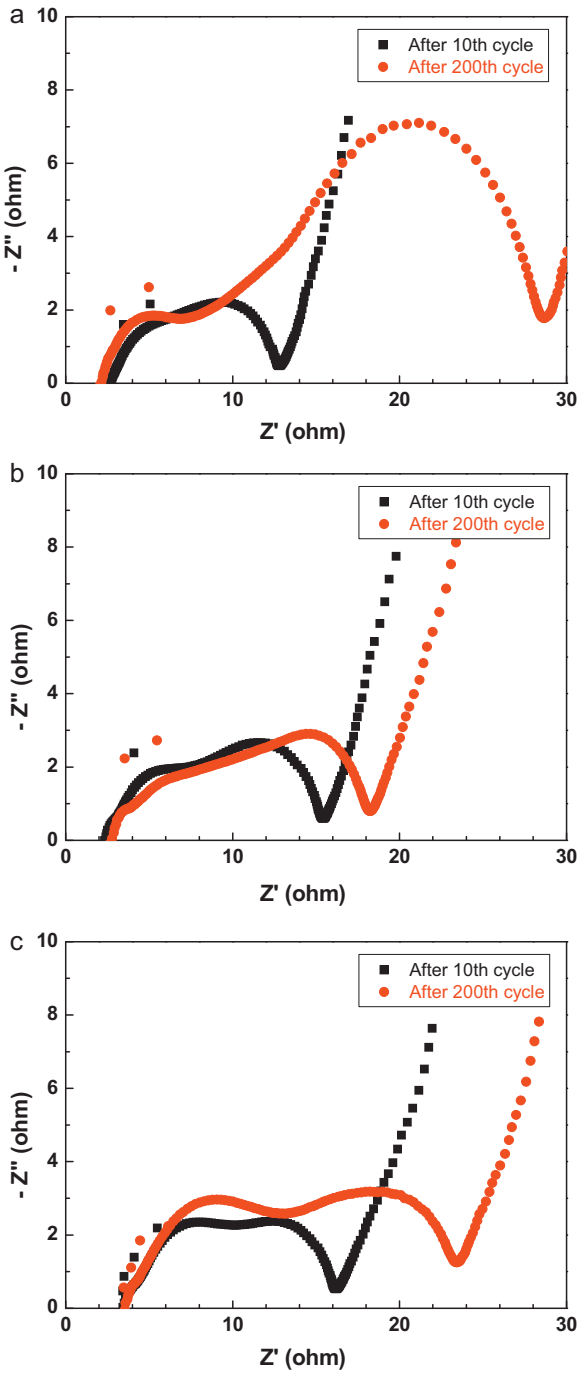

Fig. 6. AC impedance spectra of cells after the 10th and 200th cycle: (a) pristine PE separator, (b) 40 nm SiO_2-coated composite separator, and (c) 530 nm SiO_2-coated composite separator.

no decomposition of any components below 5.0 V vs. Li^+/Li takes place. This indicates that the composite separators can be a good alternative to a PE separator, even in application to high-voltage lithium-ion batteries.

The effects of the ceramic coating layers on the electrochemical performance of the composite separators were investigated as a function of SiO_2 powder size. Fig. 4 shows the discharge profiles of cells assembled with various separators. The cells were charged under a voltage range between 3.0 and 4.4 V at a constant charge current density of 0.2 C and discharged at various current densities ranging from 0.2 to 1.0 C. The voltage and discharge capacity of the cells gradually decrease with an increase of the discharge current density. No abnormal or unstable discharge profiles were observed for the composite separators. Intriguingly, the discharge capacities of the 40 nm SiO_2-coated composite separator appear to be little different from those of the pristine PE separator. This indicates that the 40-nm SiO_2 coating layer does not significantly hinder the ionic conduction, owing to its highly developed porous structure. Another important finding is that the discharge capacities of the 40 nm SiO_2-coated composite separator are higher than those of the 530 nm SiO_2-coated one. The difference in the discharge *C*-rate capacities between the composite separators becomes more pronounced at the higher discharge currents (Fig. 4(d)), where the influence of ion transport on the ohmic polarization [9] is more important. The discharge *C*-rate performance is further discussed by considering the total ionic conductance of the separators. As shown in Table 1, the total ionic conductance (=0.61 S) of the 40 nm SiO_2-coated composite separator is higher than that (=0.53 S) of the 530 nm SiO_2-coated one. This indicates that the 40 nm SiO_2-coated composite separator can afford more facile ionic transport due to its highly porous structure, which consequently could be beneficial in improving the discharge *C*-rate capability. Meanwhile, in addition to the control of SiO_2 particle size, it is also suggested that the discharge *C*-rate capability of the SiO_2-coated composite separators could be further improved by optimizing porous structure and thickness of SiO_2 coating layers. This will be definitely one of our major research interests in future studies.

Fig. 5 compares the cyclability, i.e. discharge capacity as a function of cycle number, of the composite separators with that of the pristine PE separator, where the cells were cycled under a voltage range between 3.0 and 4.4 V at a constant charge/discharge current density (0.5 C/0.5 C). An intriguing finding is that the 40 nm SiO_2-coated composite separator shows excellent discharge capacity up to 200 cycles, which appears to be slightly higher than that of the pristine PE separator. Kim and co-workers [8] reported that a ceramic layer (Al_2O_3 powders and poly(lithium 4-styrenesulfonate) binders)-coated PE separator has superior ability to retain liquid electrolytes than a hydrophobic PE separator alone, and thus helps to prevent leakage of liquid electrolyte during cycling, resulting in improved cyclability. In addition to this interpretation, in order to provide a more detailed understanding of the cycle performance of the composite separators, the AC impedance spectra of fully charged cells after the 10th and 200th cycle were analyzed in this study. Fig. 6(a) shows that the AC impedance of cells assembled with the pristine PE separator significantly increases after the 200th cycle. An increase in cell impedance is known to have a negative influence on capacity of cells [18–21]. In comparison to the pristine PE separator, the 40 nm SiO_2-coated composite separator strongly hampers the increase in the cell impedance (Fig. 6(b)). This suppressed growth in the cell impedance may be ascribed to the more intimate contact of the ceramic coating layers with the electrodes after being filled with the liquid electrolytes.

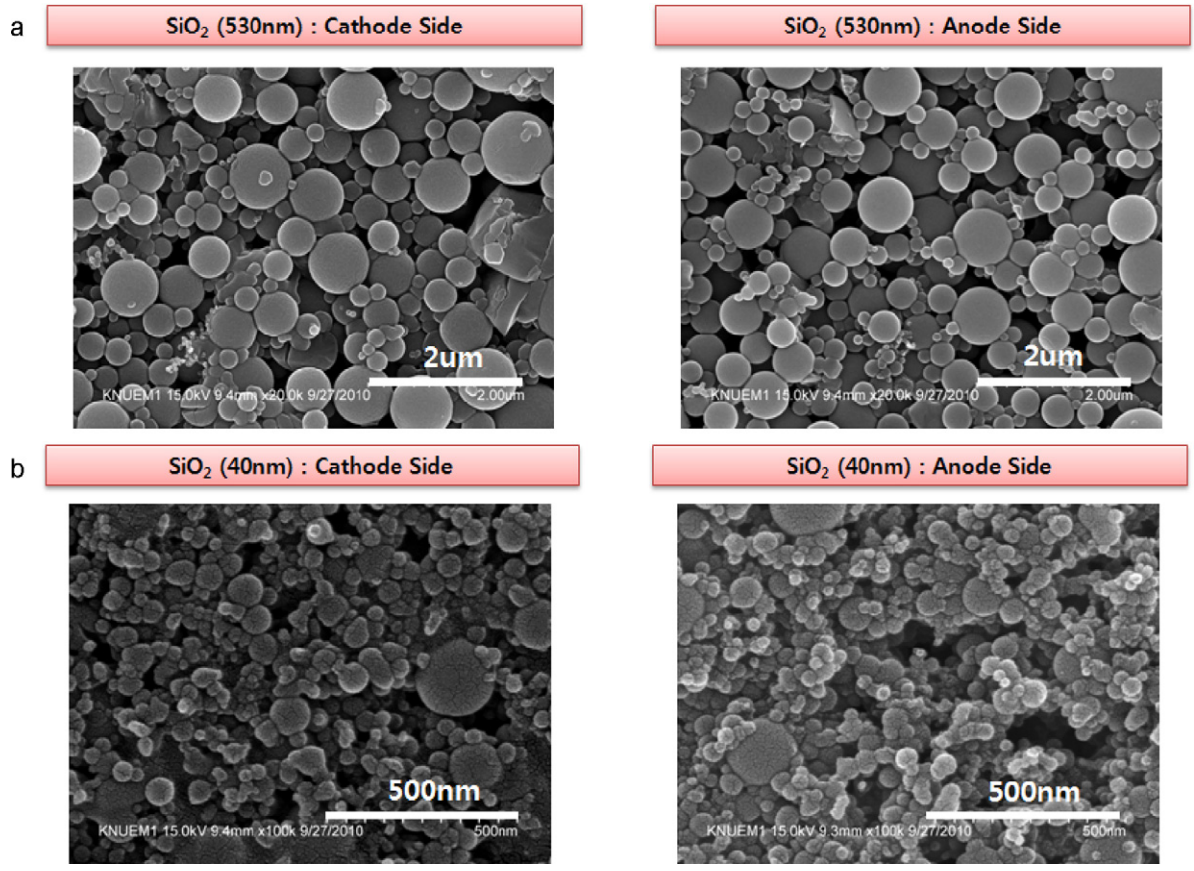

Fig. 7. Morphological characterization (surface) of SiO_2-coated composite separators after the 200th cycle: (a) 530 nm SiO_2-coated composite separator and (b) 40 nm SiO_2-coated composite separator.

A previous study [8] also reported similar interpretations on the change in AC impedance during cycling of cells assembled with various separators.

In contrast to the 40 nm SiO_2-coated composite separator, the 530 nm SiO_2-coated composite separator shows a steep decline in the discharge capacity with an increase of cycle number, resulting in the poor cyclability. The capacity retention after the 200th cycle was found to be 29% for the 530 nm SiO_2-coated composite separator, in comparison to 77% for the 40 nm SiO_2-coated one and 73% for the pristine PE separator. It has been already observed that the 530 nm SiO_2-coated composite separator has low total ionic conductance and thus poor discharge *C*-rate capability. This sluggish ion transport in the 530 nm SiO_2-coated composite separator may have a profound detrimental effect on the cyclability, even though the 530-nm SiO_2 coating layer slightly retards the growth of cell impedance (Fig. 6(c)). These results demonstrate that the SiO_2 coating layers, more specifically SiO_2 particle size, of the composite separators have a major influence on the cell performances.

Meanwhile, the morphological stability of the SiO_2-coated composite separators during cycling was examined. Fig. 7 shows that even after the 200th cycle, the SiO_2 coating layers of the composite separators are little changed at not only the cathode-contacting side but also the anode-contacting one. There has been neither breakdown of the porous structure nor peel-off of the SiO_2 nanoparticles. This intriguing result reveals that the SiO_2 nanoparticles in the coating layers are stable and hardly dissolved in the cells under this cycling condition (i.e., during 200 cycles at 0.5 C/0.5 C and 3.0–4.4 V).

4. Conclusions

We successfully developed the new composite separators by introducing the ceramic coating layers (i.e. close-packed SiO_2 nanoparticles interconnected by PVdF-HFP binders) onto both sides of the PE separators. The existence of the heat-resistant SiO_2 coating layers enabled the composite separators to show substantial reduction in the thermal shrinkage, as compared to the pristine PE separator. The effects of ceramic coating layers on the separator properties were in great detail investigated as a function of SiO_2 powder size. In comparison to the large-sized (=530 nm) SiO_2, the small-sized (=40 nm) SiO_2 presented a large number of SiO_2 nanoparticles in the ceramic coating layers, high porosity, and small increase in the cell impedance, which consequently contributed to the improvement in not only thermal shrinkage and ion transport of the separator but also cyclability of the cell. This study demonstrated that the structure control of SiO_2 ceramic coating layers plays a crucial role in determining the composite separator properties and cell performances.

Acknowledgment

This research was supported by the Converging Research Center Program through the Ministry of Education, Science and Technology (2010K001090).

References

[1] P. Arora, Z. Zhang, Chem. Rev. 104 (2004) 4419.
[2] S.S. Zhang, J. Power Sources 164 (2007) 351.
[3] G. Venugopa, J. Moore, J. Howard, S. Pendalwar, J. Power Sources 77 (1999) 34.
[4] S. Ahn, Lithium Mobile Power, San Diego, October, 2007.
[5] T.H. Cho, M. Tanaka, H. Ohnish, Y. Kondo, M. Yoshkazu, T. Nakamura, T. Sakai, J. Power Sources 195 (2010) 4272.
[6] S.S. Zhang, K. Xu, T.R. Jow, J. Power Sources 140 (2005) 361.
[7] T. Takemura, S. Aihara, K. Hamano, M. Kise, T. Nishimura, H. Urushibata, H. Yoshiyasu, J. Power Sources 146 (2005) 779.
[8] J.A. Choi, S.H. Kim, D.W. Kim, J. Power Sources 195 (2010) 6192.
[9] H.S. Jeong, D.W. Kim, Y.U. Jeong, S.Y. Lee, J. Power Sources 195 (2010) 6116.
[10] S. Augustin, V. Hennige, G. Hoerpel, C. Hying, Desalination 146 (2002) 23.
[11] T.H. Cho, M. Tanaka, H. Onishi, Y. Kondo, T. Nakamura, H. Yamazaki, S. Tanase, T. Sakai, J. Power Sources 181 (2008) 155.
[12] H.R. Jung, D.H. Ju, W.J. Lee, X. Zhang, R. Kotek, Electrochim. Acta 54 (2009) 3630.
[13] K.E. Mueggenburg, X.M. Lin, R.H. Godsmith, H.M. Jaeger, Nat. Mater. 6 (2007) 656.
[14] K.M. Kulinowski, P. Jaing, H. Vaswani, V.L. Colvin, Adv. Mater. 12 (2000) 833.
[15] C. Jiang, S. Markusya, Y. Pikus, V.V. Tsukuruk, Nat. Mater. 3 (2004) 721.
[16] M. Mulder, Basic Principles of Membrane Technology, Kluwer Academic Publishers, London, 1996.
[17] S.W. Oh, S.T. Myung, S.M. Oh, C.S. Woon, K. Amine, Y.K. Sun, Electrochim. Acta 55 (2010) 1193.
[18] K.S. Lee, Y.K. Sun, J. Noh, K.S. Song, D.W. Kim, Electrochem. Commun. 11 (2009) 1900.
[19] Y.K. Sun, J.M. Han, S.T. Myung, S.W. Lee, K. Amine, Electrochem. Commun. 8 (2006) 821.
[20] Y.K. Sun, S.W. Cho, S.T. Myung, K. Amine, J. Prakash, Electrochim. Acta 53 (2007) 1013.
[21] W. Chang, J.W. Choi, J.C. Im, J.K. Lee, J. Power Sources 195 (2010) 320.